Journal of Solid State Electrochemistry (2022) 26:591–605
https://doi.org/10.1007/s10008-021-05112-8

ORIGINAL PAPER

Effects of the composition of active carbon electrodes on the impedance performance of the AC/AC supercapacitors

Suzana Sopčić[1] · Davor Antonić[2] · Zoran Mandić[3]

Received: 19 November 2021 / Revised: 26 December 2021 / Accepted: 26 December 2021 / Published online: 10 January 2022

Abstract

Considerable diversity in the preparation methodology of active electrode materials for carbon supercapacitors makes direct comparison of the results obtained by different groups difficult. The electrode compositions usually included a variety of additives, such as the different forms of binders and/or conductive additives. All additives differ in physico-chemical properties, which affect the supercapacitive properties of electrodes in a different manner. In this study, we aimed to extend accumulated knowledge of the effect of active electrode content by performing the electrochemical characterization of a series of in-house-prepared carbon–carbon supercapacitors, which differ in compositions of active electrode materials and their thicknesses. The main focus was to investigate the frequency responses of the assembled devices and describe their behavior with the appropriate equivalent electric circuits to get a deeper understanding of the charge storage in the carbon electrodes. Assembled supercapacitors were subjected to external pressure, and the influence on cell performance was investigated. Results revealed how the applied variations influenced the equivalent serial resistance and capacitance, which is crucial in the process of supercapacitor assembly.

Keywords Symmetrical activated carbon supercapacitor · Electrochemical impedance spectroscopy · Porous electrode electric model · Equivalent serial resistance

Introduction

Electrochemical capacitors or supercapacitors gained considerable attention in the last decade of the twentieth century in the context of their feasible application in electric and hybrid electric vehicles. They were supposed to boost the power of the vehicles and efficiently utilize regenerative braking energy storage relieving the load on batteries or fuel cells. Until now, their practical applicability has spread into many other diverse areas in stationary and mobile applications.

Initial development of supercapacitors took advantage of high double-layer capacitances of electrode materials, especially carbon. It was later turned into other directions, which include the design of one or both electrodes prepared from pseudocapacitive materials [1–3]. Various metal oxides [1, 4–7] and conducting polymers [8, 9] showed promising electrochemical performances in this respect. However, despite the initial success of these materials, the lack of sufficient chemical or dimensional stabilities, reaction reversibility, and even high price hindered the mass production of corresponding symmetrical or asymmetrical pseudocapacitors. As a consequence, symmetrical activated carbon (AC) supercapacitors are now, apart from a few niche applications, almost exclusively found on the market.

Easy and cheap manufacture of highly porous carbon materials with a specific surface area well over 2000 $m^2\ g^{-1}$ leading to the specific capacitance higher than 200 $F\ g^{-1}$ is nowadays a primary reason for such domination of carbon supercapacitors. Many research efforts have been focused on the improvement of the physical and chemical properties of carbon materials to achieve high capacitances retaining low ohmic resistances. From the numerous literature reports, three main directions of the improvement of carbon materials could be distinguished: (i) selection of

✉ Zoran Mandić
zmandic@fkit.hr

[1] Institute for Medical Research and Occupational Health, Ksaverska cesta 2, Zagreb, Croatia

[2] University North, Trg dr. Žarka Dolinara 1, Koprivnica, Croatia

[3] Faculty of Chemical Engineering and Technology, University of Zagreb, Marulićev trg 19, Zagreb, Croatia

appropriate carbon materials and their chemical or electrochemical activation [10–17], (ii) using different methods of preparation to achieve desired specific area and optimal distribution of pore sizes [18, 19] and (iii) modification of the carbon surface with different organic and inorganic materials to tailor their pseudocapacitive properties [5, 20, 21]. In all these cases, the key target was the optimization of the size of the pores and their distribution to achieve good mobility of the ions inside the pores. A good correlation between the pore sizes and electrolyte ions' size is crucial for supercapacitor performance [1, 22–28]. Additionally, it was demonstrated that in some cases, a partial or complete desolvation of ions is needed before their migration into the porous structure of carbon [1, 23, 24, 29, 30], and thus, the strength of the solvation shell of the ions needs to be taken into account when selecting appropriate solvent [31]. Thus, a good estimate of a Gibbs free energy is needed [32] and possible chemisorption of ions [33].

Another important aspect of supercapacitor design and its performance is the preparation of the active electrodes and assembly of the device. Supercapacitor electrodes are usually prepared in a similar manner as many other electrode materials for electrochemical power sources, especially those utilized in Li-ion battery technologies. However, there are only a few papers addressing the issue of the influence of the methods of preparation and electrode composition on the electrochemical properties of the carbon supercapacitors [34–38]. To avoid deterioration of electrode materials and boost supercapacitor performance, slight amounts of different additives that address shortcomings or improve various functionalities are added in several weight-percent in both electrode composition and electrolyte. Electrodes are usually prepared in the form of a mixture of active carbon, conducting additives such as carbon black, and a small amount of binder. Generally, active carbon as active electrode mass is mixed with conductive additive at a level high enough to reach the percolation threshold to ensure low resistance pathways for electrons from the current collector side to the solid/solution interface. The mechanical integrity of the electrodes is provided by a binder, usually a polymeric material, most commonly being poly(tetrafluoroethylene) (PTFE), poly(vinylidene fluoride) (PVDF), and hydroxymethyl cellulose (HMC). The role of the binder is to allow good mechanical integrity of the electrode by forming a compact three-dimensional porous layer with good interparticle connections and good adhesion of the particles to the current collector [39, 40]. Both are of vital performance in the supercapacitor design to minimize ohmic resistance and to achieve extended cycle life and high power ratings. Binder should possess high chemical and electrochemical stability, chain flexibility, and low solubility in the solvents used in the devices [36].

While ensuring the integrity of the carbon electrode, polymeric binders tend to block the porous structure of the electrode, decreasing the active surface for ion adsorption and consequently decreasing the gravimetric capacitance [35]. Another property of polymeric binders which might influence the capacitance of carbon electrodes is their hydrophobicity which effectively repulses the electrolyte ions from entering into the electrode layer [34]. In this context, more hydrophilic polymeric binders [41] or water-soluble binders [38, 42] might exert a positive influence on the overall performance of the supercapacitors. On the other hand, the additives should fulfill their primary function and their overall content should be optimized carefully to achieve maximum performance of the device. Usually, the contents of the additives vary between 5 and 10% but there is a very limited number of studies that dealt with the effect individual components exert on the behavior of the electrode materials, supercapacitor charge storage, and power capabilities.

The beneficial effects of various components are still poorly understood, and conflicting results about their influence on the supercapacitor performance could be found in the literature. In addition, it is very difficult to establish a clear relationship between the composition of the electrodes and their performance since in a three-component mixture containing active carbon, binder, and conductive additive, it is not possible to vary the fraction of a single component while keeping fixed fractions of other components. To complicate things further, it was demonstrated that it is not only the composition of the electrode that affects the final performance of the supercapacitor but also the procedure of the components mixing and the preparation of electrodes [15]. Such sensitivity of the carbon electrode behavior and later supercapacitor performance on the preparation conditions make the comparisons of the results obtained by different research groups difficult. As a rule of thumb, improving some properties of carbon electrodes by the addition of additives usually leads to the deterioration of other properties. Consequently, the optimal composition of the electrode should be found for tailoring its properties for a particular application.

Herein, we describe the electrochemical characterization of a series of in-house-prepared carbon–carbon supercapacitors, which differ in compositions of active electrode materials and their thicknesses. The main focus was to investigate the frequency responses of the assembled devices by the electrochemical impedance spectroscopy measurements (EIS). EIS is a proven method for the characterization of supercapacitors and determination of their deviation from ideality which usually manifests as a frequency dependence of capacitance [43–45] and, as such, might provide a useful methodology for identifying the roles of various components of carbon electrodes. Although there are numerous studies investigating the frequency behavior of the carbon

electrodes and supercapacitor cell performance, EIS was not used extensively and systematically to probe the sensitivity of impedance response on the minute changes in the carbon electrode compositions.

The non-ideal behavior of supercapacitors is usually ascribed to the distributed electrical features of the porous electrodes. The concept of porous electrodes was introduced by de Levie [46], who showed that the impedance down the cylindrical pores could be modeled by the simple R–C transmission line model (Fig. 1) defined by Eq. (1).

$$Z_s(\omega) = R_s(i\omega\tau_s)^{-\rho} coth R_s(i\omega\tau_s)^{\rho} \quad (1)$$

where R_s represents electrode resistance inside the pores, ω angular frequency, τ_s time constant, and exponent p, a coefficient which describes the deviation of capacitance values from ideality. For ideal systems, p is 0.5, and for non-ideal systems, capacitor is replaced by the constant phase element (*CPE*) having $p < 0.5$.

Under the assumption of negligible resistance of the solid electrode compared to the electrolyte resistance within pores, R_s and $C_s = \tau_s / R_s$ represent the total electrolyte resistance and total double-layer capacitance inside the pores.

Experimental

Preparation of electrode materials and assembly of supercapacitors

The electrode materials were prepared by mixing various weight percentages of activated carbon (Norit DLC Supra 30, $S_{BET} = 1900\ m^2\ g^{-1}$), carbon black (Timcal Super C45), and PVDF (Sigma Aldrich). The properties of the active carbon used in this work were described elsewhere [47]. Table 1 shows the compositions of selected electrodes presented in this paper. After weighting, all three components were mixed for 30 min by Vortex mixer (Neautrion) to obtain a uniform powder mixture. By adding N-methyl-2-pyrrolidone (NMP) (Sigma Aldrich) solvent, the slurry texture was achieved. After homogenization, the slurry was coated onto a commercially available Al-foil current collector covered with a 1-µm carbon micro-thin layer (Galon) with the help of a thin layer coater (Gelon Lib Group) which produced a uniform electrode thickness. After coating, foil sheets were dried overnight at 60 °C in the vacuum furnace. Dried electrodes were cut into a circular shape of 2 cm^2 and hot-pressed at 80 °C and 100 MPa. Mass loadings of the prepared electrodes varied from 2.8 to 27.6 mg cm^{-2} depending on the electrode thickness from 60 to 210 µm, respectively. Before supercapacitor assembly, the electrodes were dried overnight in the vacuum oven at 120 °C to remove traces of water.

Table 1 Electrode compositions of the prepared supercapacitors

Supercapacitor	*w (activated carbon) /%*	*w (carbon black)/%*	*w (PVDF)/%*
SC1	90	5	5
SC2	80	15	5
SC3	80	10	10
SC4	60	20	20

Supercapacitors were assembled inside the MBraun argon-filled glove box (O_2, H_2O below 1 ppm). The glass fiber separator (250 µm, MN GF-5, Macherey–Nagel) was embedded between two electrodes of the same thickness and mass loading. The electrode/separator assembly was inserted into the chemically and mechanically resistant polymer (polyethylene terephthalate/aluminum/polyethylene)–coated Al foil with implemented Al contacts for each electrode. The separator was soaked with 0.25 M tetraethylammonium tetrafluoroborate ($TEABF_4$) in acetonitrile (ACN), vacuumed, and sealed to prevent electrolyte evaporation. The choice of $TEABF_4$/ACN was based on the numerous results which demonstrated its superiority over other electrolytes for supercapacitor applications in terms of electrolyte and pore resistances, capacitance, and the working temperature range [48–53].

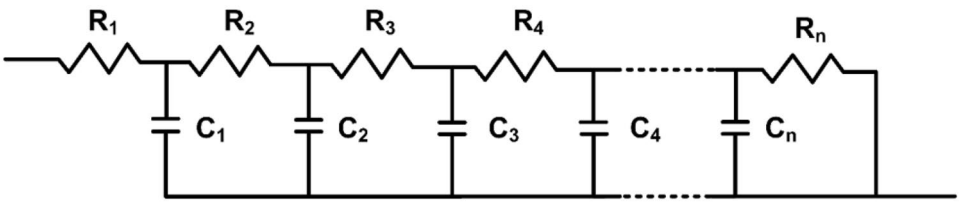

Fig. 1 Scheme of R–C transmission line model for porous electrodes. The total resistance of porous electrode is defined as $R_s = R_1 + R_2 + R_3 + R_4 + R_n$, while the total double-layer capacitance of porous electrode is defined as $C_s = C_1 + C_2 + C_3 + C_4 + C_n$. The number of *R* and *C* elements depends on the pore length

Electrochemical testing of supercapacitors

Electrochemical and capacitive properties of assembled supercapacitors were characterized by cyclic voltammetry (CV), electrochemical impedance spectroscopy (EIS), and galvanostatic charging/discharging method (GCD) using SP-200 Biologic potentiostat–galvanostat supported by EC-Lab software.

Before measurement, the supercapacitor was placed between two plates and tightened with controlled pressure in the range of 5–100 MPa. CV was recorded in a voltage range from 0 to 2.5 V with a scan rate of 50 mV s^{-1}. The galvanostatic charging/discharging method was performed according to the supercapacitor testing standard [54]. GCD was carried out in a five-step procedure within 50–100% of the nominal voltage value between 1.25 and 2.5 V (Fig. 2). The testing procedure consisted of the following steps: supercapacitor was held at an open-circuit voltage (OCV) for 10 s (**1**); charged by the constant current to nominal voltage, U_r (2.5 V) (**2**); held at the nominal voltage for 30 s (**3**); left at the OCV voltage another 10 s (**4**); and then discharged by the constant current to the voltage value of 1.25 V (U_1) (**5**). The charging and discharging processes were performed with the constant current of 0.63 to 1.65 A g^{-1}, depending on the electrode thickness.

Capacitance, C (F), of assembled supercapacitor was calculated according to Equation (2) [54]:

$$C = \frac{2W}{\left[\left(0.9U_r\right)^2 - \left(0.7U_r\right)^2\right]} \tag{2}$$

where W is the measured discharged energy (J) in the voltage range used of 0.9 U_r to 0.7 U_r and U_r is the nominal voltage the supercapacitor is charged (2.5 V).

Energy, W (J) is calculated from Eq. (3):

$$W = \int_{t_0}^{t_{Ur}} I_d U(t) dt \tag{3}$$

where I_d is discharging current (A), t (s) is the time of supercapacitor discharge, and U (V) is voltage change during supercapacitor discharge.

Equivalent serial resistance, ESR (Ω), is determined by the least squares internal resistance method according to Eq. (4) [54]:

$$ESR = \frac{\Delta U_r}{I_d} \tag{4}$$

where I_d is the discharge current (A) and ΔU_r is the voltage drop at the start of the discharge (V). In Fig. 2, this voltage drop can be seen at the beginning of the 5th testing step of the charging/discharging procedure.

The EIS measurements were carried out with a sinusoidal signal of 10 mV in amplitude over a frequency range of 1 MHz to 0.01 Hz and with 6 measured points per decade. All measurements were made on three freshly prepared electrodes and recorded in triplicate to identify the stability of the system and to confirm the reproducibility. Precautions were made to avoid possible measurement artifacts that could appear in these systems [48, 55, 56]. Impedance data were fitted with the Z fit module of EC-Lab, Ver 11.18 (Bio-Logic), and ZView software (Scribner associates). The complex non-linear least squares (CNLS) method was used to fit the experimental data. The fit was considered acceptable when the statistical parameter goodness of fit, χ^2, was lower than 10^{-4}. Simulated data were critically evaluated to avoid possible misinterpretations with artificial effects [57, 58].

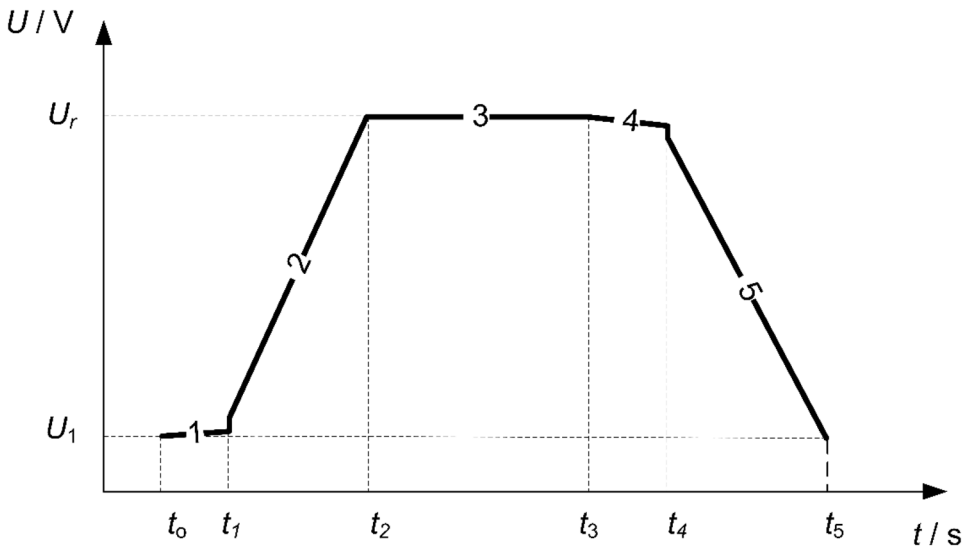

Fig. 2 Schematic view of the charging/discharging five step testing procedure. U_1 (V) represent the starting voltage and U_r is a nominal voltage ($U_1 = 0.5 \times U_r$)

Results and discussion

Cyclic voltammograms of all prepared supercapacitors show qualitatively similar behavior and exhibit close to an ideal rectangular shape as would be expected for good capacitive materials. Figure 3a shows the selection from the first 30 cyclic voltammetric cycles of the SC1 supercapacitor. The first cycle effect is evident as the increased voltammetric current over the whole potential range, attributed to the non-steady-state spatial distribution/redistribution of charge within the depth of the pores. Charge redistribution is a well-known phenomenon that affects the voltages of the supercapacitor and is the primary reason for the supercapacitor self-discharge [59, 60]. However, after the first few cycles, the cyclic voltammetric response achieves reproducible, reversible, and almost ideal behavior.

GCD curves obtained for the continuous charging/discharging of the SC1 supercapacitor are shown in Fig. 3b. Again, the first charging cycle differs from the rest of the cycles where the voltage profile assumes stable steady-state behavior. In this case, charge redistribution within the pores is also evident in the voltage decay observed when the supercapacitor is left at open-circuit potential between approximately 55 and 65 s. Voltage decay is caused by the supercapacitor self-discharge and is becoming less pronounced with the number of GCD cycles. Self-discharge equivalent resistance, calculated from the R–C time constant obtained from the self-discharge voltage profile, in the first cycle was 1.1 kOhm stabilizing at 2.1 kOhm in the 30th and subsequent cycles.

From the GCD curves, *C* and *ESR* could be determined according to Eqs. (2) and (4), respectively. Dependences of these parameters on the number of cycles during the first 30 consecutive cycles are shown in Fig. 4a and b. The aim of these measurements was to test the stability of the supercapacitor performance during the concomitant impedance studies and not to investigate the long-term stability of the supercapacitor electrodes. Figures show stabilization of supercapacitor behavior after only a few cycles of charging and discharging. *ESR* value decreases from 2.299 to 2.184 Ω, meaning that ions that participate in the charging/discharging process have established their path throughout the pores and their transport has improved. The capacity value decreased as it was explained because of the 1st cycle effect, and the value of 0.38 F remains almost constant through the remaining charging/discharging cycles. It is important to point out that all impedance results shown in this paper do not differ to a significant extent if taken before and after these 30 cycles.

Dynamic electrical behavior of assembled carbon–carbon supercapacitors was evaluated using electrochemical impedance spectroscopy. The typical spectra represented as Nyquist and Bode plots for as assembled SC1 supercapacitor before subjecting it to the CV and GCD testing procedures are shown in Fig. 5.

On the impedance plots, four distinct regions can be observed. In the low to intermediate frequency range (up to 100 Hz), typical capacitive behavior of porous electrodes was observed consisting of Warburg-type region at higher frequencies (1–100 Hz, region III) represented by close to

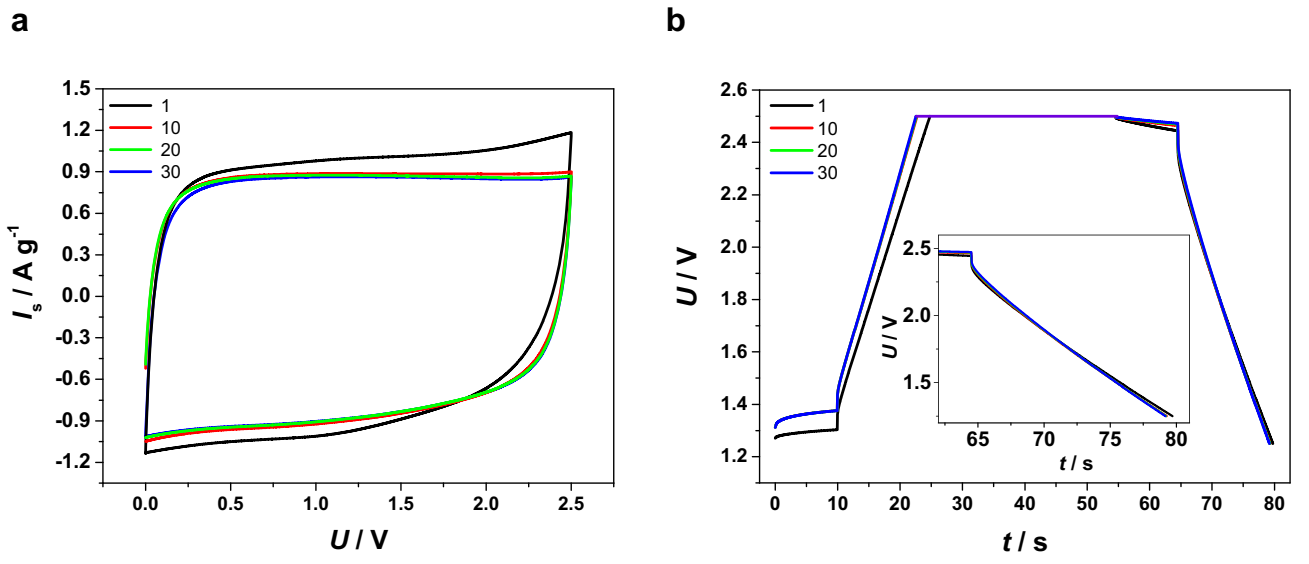

Fig. 3 Capacitive behaviour of SC1 supercapacitor **a** cyclic voltammograms recorded in the voltage range from 0 to 2.5 V at scan rate of 50 mV/s for 30 cycles; **b** charging/discharging curves performed in the voltage range of 1.25 to 2.5 V with constant current of 1.16 A g^{-1} recorded for 30 cycles

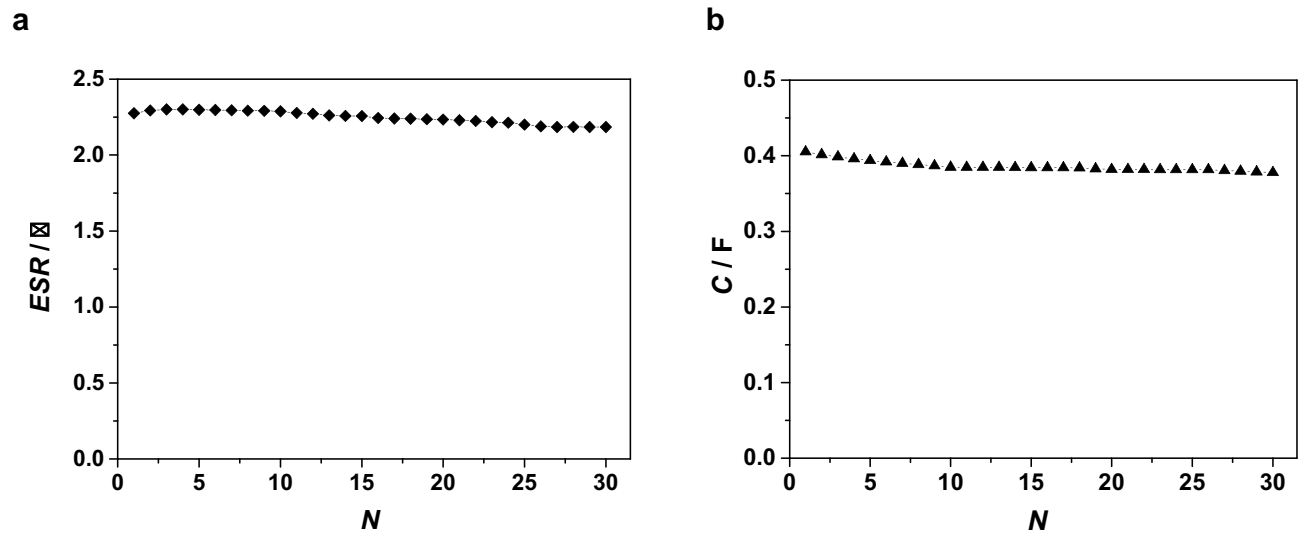

Fig. 4 **a** Equivalent serial resistance and **b** capacitance of SC1 supercapacitor calculated from discharge curves obtained by constant current of 1.16 A g^{-1}. The parameters were calculated according to Eqs. (2) and (3). *N* represents the charging/discharging cycle

ideal − 45° slope followed by the almost pure capacitive response at lower frequencies (0.01–1 Hz, region IV). Such behavior for supercapacitors has been well documented in the literature [43, 45, 61, 62].

At the frequencies higher than 50 kHz (region I), the impedance data turned from negative to positive slope, and in this region of frequencies, the inductive behavior of the supercapacitor dominates. The inductance, in this case, is not related to the electrochemical processes inside the supercapacitor device, but rather, it is considered as a stray inductance usually observed in highly conducting battery and supercapacitor cells being caused mainly by cables and cell connections [63]. However, during simulation and fitting of the experimental impedance data, it is important to take inductance into account to obtain an accurate determination of the cell electrical parameters, especially high-frequency resistance (R_{HF}), which directly influence the value of equivalent series resistance (*ESR*), one of the key parameters describing supercapacitor performance. In systems without inductive elements, R_{HF} is readily determined as an extrapolation of the high-frequency limit of impedance data.

The transition from the high-frequency inductive behavior to the middle-to-low-frequency capacitive behavior of the porous electrodes goes through the frequency range where

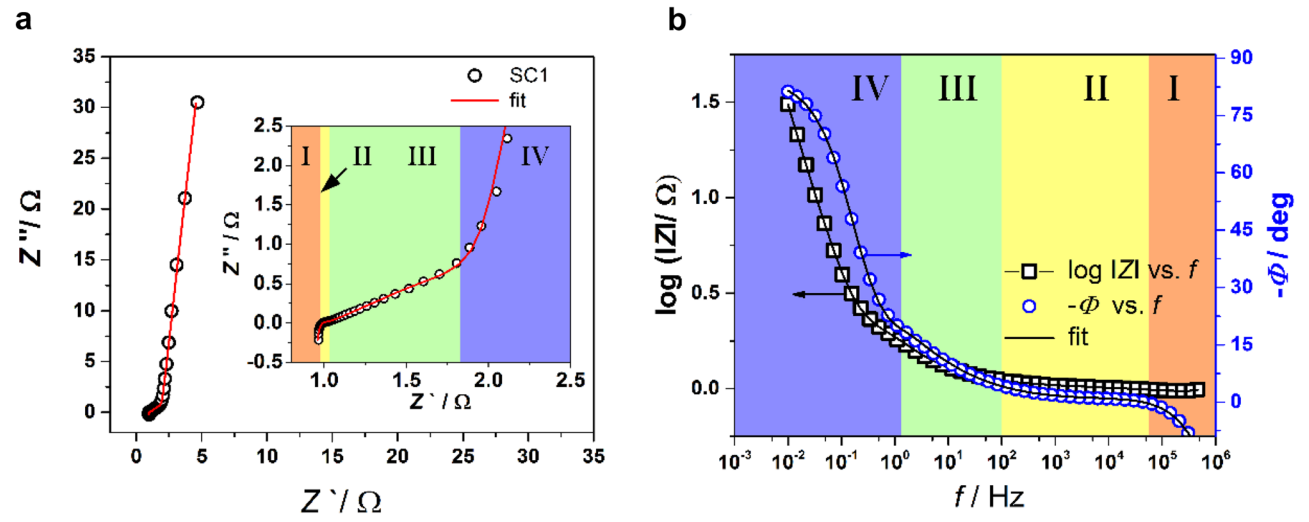

Fig. 5 **a** Nyquist diagram; **b** Bode diagram for SC1 supercapacitor both with fitting results recorded in the frequency range of 1 MHz to 0.01 Hz, DC potential of 0 V and sinusoidal signal of 10 mV in amplitude. External tightening pressure of 100 MPa was applied to a supercapacitor. Nyquist diagram inset magnifies the data in the high-frequency range

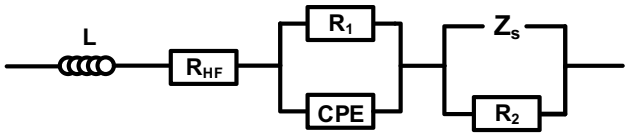

Fig. 6 Equivalent electric circuit used for mathematical modelling of impedance response of assembled supercapacitors

semicircle impedance in Nyquist plots could be observed to the higher or lesser extent depending on the tested supercapacitor device (region II). In contrast to the low-frequency capacitive or high-frequency inductive behavior, the appearance of the semicircle in the impedance plots indicates the existence of the kinetic processes usually associated with one of the interphases and is prone to appear in both batteries and supercapacitors. It is usually assigned to either carbon/electrolyte or carbon/current collector interfaces [43, 64, 65].

Thus, the impedance spectra shown in Fig. 5 could be modeled by the equivalent circuit shown in Fig. 6.

In the equivalent circuit model, L represents high-frequency inductance, R_{HF} high-frequency resistance, R_1/CPE parallel combination related to the kinetic process taking place at one of the interphases, Z_s element represents the impedance related to the "open" R–C transmission line model described by Eq. (1), and R_2 is resistance due to the charge leakage at the electrode/solution interface leading to the self-discharge of the supercapacitor device. The total impedance of the system can thus be described by Eq. (5):

$$Z(\omega) = Z_L(\omega) + R_{HF} + Z_{RC}(\omega) + (Z_S(\omega)R_2)/ + (Z_S(\omega) + R_2) \quad (5)$$

In the impedance $Z_{RC}(\omega)$, the constant phase element (CPE) is used to fit the data to account for the non-ideality of the surface reactions due to different surface inhomogeneities. Surface inhomogeneities arise in the porous electrodes usually due to the distribution of energies of active sites at the electrodes caused by the porous structure of the material, different spatial arrangements of the electrode components, or others [43, 66–68]. The total resistance of such supercapacitor systems is defined by the equivalent serial resistance (ESR) composed of all resistances present in the supercapacitor (Eq. 6).

$$ESR = R_{HF} + R_1 + R_s(\omega) + R_2 \quad (6)$$

Fitted values of the equivalent circuit parameters for the spectrum shown in Fig. 5 are given in Table 2.

As indicated in the table, the leakage resistance, R_2, was too high to be determined for the results presented in Fig. 5 and most of the following results presented in this paper. Apart from the charge transfer reactions at the carbon/electrolyte interface, supercapacitor self-discharge is to its greatest extent caused by the charge redistribution within the porous structure of carbon electrodes [59, 60].

To further investigate charge storage in carbon electrodes and to determine how the external conditions, as well as the composition and preparation of electrodes, affect the performance of assembled supercapacitors, impedance measurements were conducted at variable external pressures applied to the whole cell, four different electrode compositions over four electrode thicknesses.

Effect of external pressure on supercapacitor response

It was already demonstrated in several papers that external pressure applied to the electrochemical cell could significantly affect its electrical and electrochemical characteristics. It is equally valid for lithium-ion batteries [69, 70] and supercapacitors [43, 65, 71]. In this paper, the influence of the external pressure in the range of 5–100 MPa applied on the supercapacitors of different electrode compositions during measurement was tested. The impedance responses in all cases exhibited the change in the high-frequency range of the spectra, while the low-frequency range remained largely unaffected. Figure 7 shows impedance spectra for two selected assembled supercapacitors of different electrode compositions. Both supercapacitors show general features which can be modeled by the equivalent circuit from Fig. 6. The relative insensitivity of the low-frequency region on the applied pressure is visible on the full figures indicating that the applied pressure does not affect the porous structure of the electrodes and their capacitances. Although the decrease of porosity could be expected due to blocking of the surface area of the particles by the binder and its hydrophobicity, the low-frequency data demonstrate that

Table 2 Fitting results of impedance spectra for SC1 supercapacitor using equivalent circuit model shown in Fig. 6. CPE-τ and CPE-p represent the parameters that mathematically describe the CPE element while R_S, Z_S-τ, and Z_S-p represent the Z_s element in the model

	L/H e-8	R_{HF}/Ω	R_1/Ω	CPE-τ/Ss^p	CPE-p	R_S/Ω	Z_S-τ/s	Z_S-p	R_2/Ω	χ^2
SC1	7.99	0.938	0.081	0.0124	0.523	2.664	1.211	0.473	n/m*	2.4 e-4
Error (%)	2.6	1.7	22.0	61.9	15.7	0.76	0.99	0.17	-	

*Not measurable—too high to be determined

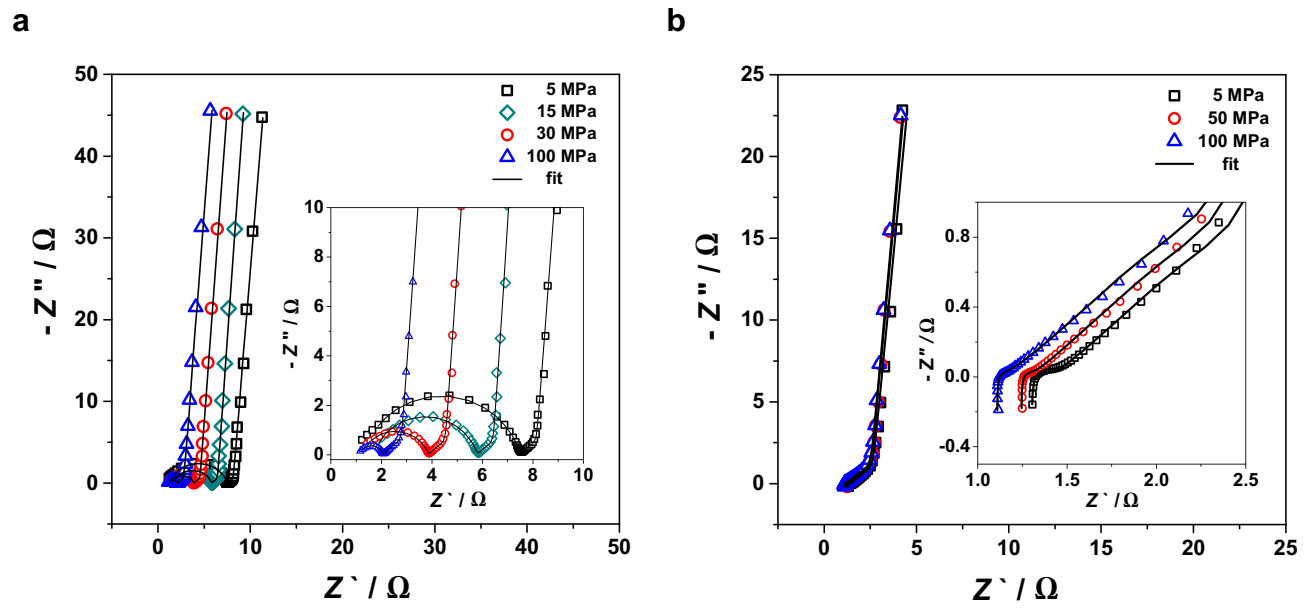

Fig. 7 Nyquist diagrams of **a** SC2 supercapacitor when external pressure of 5, 15, 30, and 100 MPa was applied; **b** SC3 supercapacitor at applied pressure of 5, 50, and 100 MPa. Solid lines represent the fitting results

during the preparation of the electrodes a complete wetting of carbon surface throughout the interior of the pores was successfully done and that the microporous surface area was not affected, at least not in the significant amount, by the variation of the electrode composition. This is in contrast to the work of Wei et al. [71], who demonstrated that specific capacitances of the CNT supercapacitors increase with the increase of pressure due to the improved wettability of CNT electrodes. However, similarly to their work, in the high-frequency range (Fig. 7a and b insets), the changes of the two resistive components (R_{HF} and R_1) are prominent. For the supercapacitor SC2 (Fig. 7a), the pressure effect is mainly reflected through the size of the depressed semicircle which represents slow interfacial kinetics (R_1/*CPE*). The size of the real part of the semicircle reversibly follows applied pressure from about 6.5 Ohm at 5 MPa to about 1 Ohm at 100 MPa. Supercapacitors assembled from the electrodes of different compositions show similar responses to the applied pressure but the extent to which the pressure affects R_{HF} and R_1 resistive components differs. Figure 7b shows the impedance diagram in the full frequency range and in the high-frequency region (inset) for the supercapacitor SC3. In this case, the increase of the pressure leads to a more significant drop of R_{HF} and *ESR*, while the kinetic semicircle vanishes completely at pressures higher than 5 MPa. It is worth noting that there is no noticeable change of the impedance spectra before and after applying pressure indicating that no mechanical damage was caused to the electrodes. These results prove that the pressure applied after the assembly of a device is of equal importance as the pressure applied to the electrodes after electrode preparation but before the assembly [36, 65].

These results demonstrate the complex influence of the electrode compositions on the electrochemical behavior of supercapacitors. Kinetic effects observed at the semicircle frequency ranges could be attributed either to the processes at the current collector/electrode or to the processes at solid/liquid interphase. The electrode process at the solid/liquid interphase would inevitably involve charge transfer leading to the chemical reaction of electrolyte and transformation of the electrode surface. Since they were not observed during the prolonged operation of the supercapacitors and since the low-frequency region of the impedance data was not affected, the kinetic semicircle was assigned to the current collector/electrode solid/solid interface. Both interfaces are very important for the proper and efficient operation of supercapacitors since the solid/liquid interface must ensure very high surface area and non-hindered influx and efflux of ions. On the other hand, contact resistance represented with the R_1 element in Fig. 6 adds up to the *ESR*-limiting high-rate capabilities of supercapacitors and for the construction of the high-power supercapacitors, contact resistance between active electrode materials and current collector should be minimized as much as possible. The role of the binder is to make a good connection among carbon particles forming a compact and porous framework and at the same time ensuring good adhesion of the carbon particles to the current collector. However, as demonstrated in a number of papers [15, 35, 36, 65], specific capacitances tend to decrease with an increasing binder content due to blocking

Table 3 Parameters obtained by mathematical fitting of impedance spectra for SC2 supercapacitor at different applied pressures. *CPE-τ* and *CPE-p* represent the parameters that mathematically describe the *CPE* element, while R_S, Z_S-*τ*, and Z_S-*p* represent the Z_S element in the model

Pressure/MPa	***L***/H e-8	R_{HF}/Ω	R_1/Ω	***CPE-τ***/Ss^p	***CPE-p***	R_S/Ω	Z_S-*τ*/s	Z_S-*p*	R_2/Ω	χ^2
5	-	1.28	6.21	4.28 e-6	0.83	1.90	0.58	0.4	n/m*	2.78 e-4
Error/%	-	1.2	0.3	4.0	0.4	3.4	3.8	0.2	-	
15	-	1.83	3.97	4.60 e-6	0.83	1.84	0.56	0.480	n/m*	2.12 e-4
Error/%	-	0.93	0.49	5.04	0.52	2.30	2.57	0.13	-	
30	-	1.22	2.64	8.07 e-6	0.79	1.94	0.59	0.479	n/m*	4.02 e-4
Error/%	-	0.92	0.53	6.77	0.68	2.37	2.71	0.17	-	
100	-	1.12	0.94	1.06 e-5	0.83	2.13	0.65	0.478	n/m*	3.83 e-4
Error/%	-	0.74	1.01	11.75	1.13	1.39	1.67	0.15	-	

*Not measurable—too high to be determined

of pores by hydrophobic chains and, consequently, a trade-off should be made between capacitance and Ohmic resistance when designing a supercapacitor. The optimal composition will depend on the particular application, i.e., whether high power is required from a device, in which case a higher content of a binder is desirable or the energy content related to the capacitance is more important.

The results obtained in this work show that the binder is even more important for the overall conductivity of electrode material than carbon black as a conductive additive. Although the content of CB was decreased in supercapacitor SC3 (Fig. 7b) compared to the supercapacitor SC2 (Fig. 7a), the simultaneous increase of the content of PVDF from 5 to 10% has a more profound influence on the observed resistances, especially on R_1. The PVDF content of 10% is considered optimal in the context of this work. This value seems to be binder-specific since different values could be found in the literature. For example, the PTFE binder yields optimal content of 5% [34], and Nafion as a binder shows the insensitivity of capacitance on its content in the range of 10–30% [41]. The result of 10% optimal content of PVDF is in accordance with the results of Daraghmeh et al. [36], who investigated carbon nanotube electrodes with PVDF as a binder, although in their case, electrode capacitances were more sensitive on the actual composition.

Fitted parameters for impedance diagrams shown in Fig. 7a are given in Table 3 and for diagrams shown in Fig. 7b in Table 4.

Effect of the electrode composition

The effect of the electrode composition on the supercapacitor performance has already been partially demonstrated in the previous paragraph during studies of the effect of the pressure on supercapacitor performances. We further investigated a series of compositions of the electrodes ranging from 60 to 90% of active carbon and 5–20% of both additives, carbon black, and PVDF. Figure 8a and b shows the selection of the impedance graphs of the four different electrode compositions for two different electrode thicknesses. The observed effects are complex and reflected in both the low-frequency capacitive range and in the high-frequency kinetic region. The complete relationship of the performance of the multicomponent system and its composition is difficult to establish experimentally since the change of the fraction of one component in the mixture automatically changes the fraction of others which might have the same or opposing effect. However, general conclusions could be drawn from the experimental results.

From the obtained results, two main trends could be discerned. While R_{HF} remains largely insensitive to the electrode composition, the diameter of the kinetic semicircle increases, and low-frequency capacitance, which is inversely proportional to the imaginary impedance, decreases with decreasing content of active carbon. The decrease of a low-frequency capacitance with a decrease of the active carbon content is expected but less clear is the effect of other

Table 4 Parameters obtained by mathematical fitting for impedance spectra of SC3 supercapacitor at different applied pressures. *CPE-τ* and *CPE-p* represent the parameters that mathematically describe the *CPE* element, while R_S, Z_S-*τ*, and Z_S-*p* represent the Z_S element in the model

Pressure/MPa	***L***/H e-8	R_{HF}/Ω	R_1/Ω	***CPE-τ***/Ss^p	***CPE-p***	R_S/Ω	Z_S-*τ*/s	Z_S-*p*	R_2/Ω	χ^2
5	5.89	1.292	0.142	0.0174	0.545	3.441	2.215	0.473	n/m*	2.78 e-4
Error/%	5.86	0.88	10.45	67.00	13.73	1.46	1.85	0.28	-	
50	6.45	1.237	0.070	0.0516	0.516	3.552	2.287	0.475	n/m*	2.12 e-4
Error/%	3.97	0.73	17.03	98.44	22.02	1.08	1.37	0.21	-	
100	6.79	1.1	0.087	0.336	0.384	3.847	2.48	0.474	n/m*	4.02 e-4
Error/%	3.16	0.80	19.22	71.93	24.53	1.16	1.41	0.219	-	

Not measurable—too high to be determined

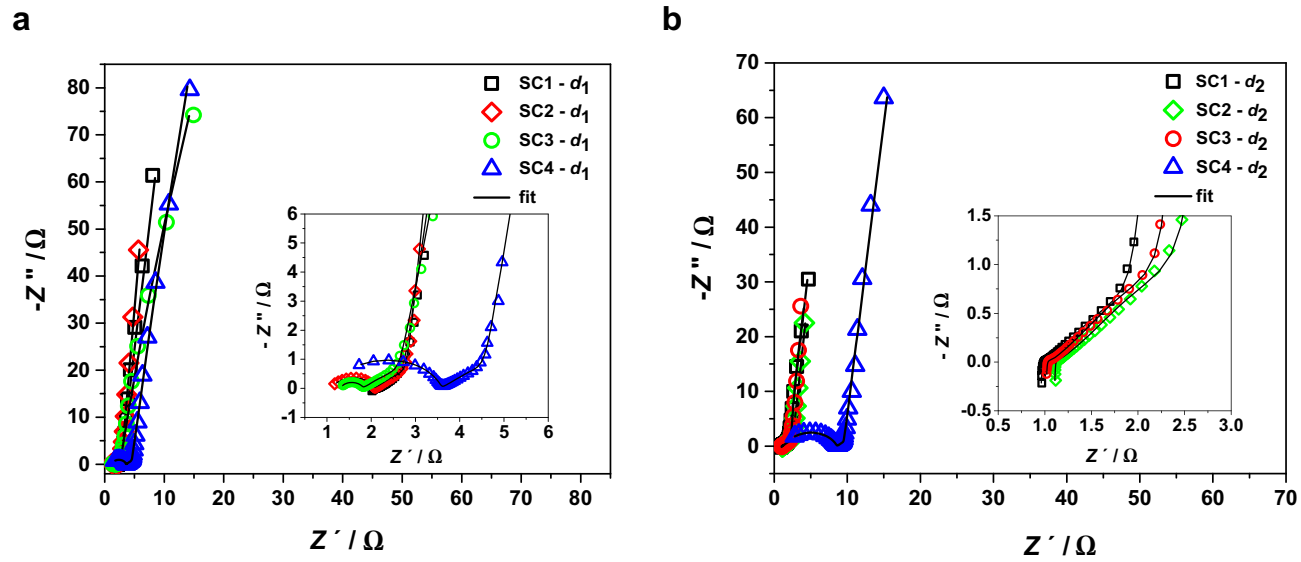

Fig. 8 Nyquist diagrams of assembled supercapacitors with different electrode composition but similar electrode thicknesses of **a** $d_1 \sim 70$ µm; **b** $d_2 \sim 120$ um. Solid lines represent the fitted results

components on the capacitances. It seems that the binder (PVDF) has a negative influence on the capacitance of the electrode because its chains envelop the active carbon particles interfering with the ion transport within the porous structure of the electrode.

As the high-frequency kinetic region is concerned, the observed resistance confirms the earlier observation that the registered semicircle is the result of a slow charge transfer between the current collector and electrode active particles. As the content of active carbon is increased, the kinetic semicircle diminishes, and for higher thicknesses of the layer and active carbon content equal or higher than 80%, the R_1 disappears completely, and only the Warburg region could be identified at high frequencies (Fig. 8b inset).

The impedance graphs are slightly shifted along the x-axis depending on the composition, indicating the R_{HF} also varies among the investigated electrodes. The order of the shift of the curves does not follow the simple order of CB content, indicating that both CB providing conductive paths through the electrode layer and PVDF providing mechanical integrity of the electrode improving interparticle contacts play an important role in ensuring good conductivities of the layers. Also, these results indicate that the charge transfer at the current collector/active material interface occurs via the electron exchange with the active carbon and the electron transfer to carbon black could be neglected.

The results demonstrate that it is difficult to establish a clear-cut relationship between the content of a single component and supercapacitor performance since varying the fraction of a single component while keeping fixed fractions of other components is not possible. Thus, before the construction of supercapacitor is approached, its intended application should be first considered since the optimal electrode composition might depend on it.

Fitted parameters for impedance diagrams shown in Fig. 8a and b are given in Tables 5 and 6.

Table 5 Results of mathematical fitting of impedance spectra of assembled supercapacitors with different electrode compositions and similar electrode thickness of $d_1 \sim 70$ µm. *CPE-τ* and *CPE-p* represent the parameters that mathematically describe the *CPE* element, while R_S, Z_S-τ, and Z_S-*p* represent the Z_S element in the model

	L/H e-8	R_{HF}/Ω	R_1/Ω	*CPE-τ*/Ss^p	*CPE-p*	R_S/Ω	Z_S-τ/s	Z_S-*p*	R_2/Ω	χ^2
***SC1-d*$_1$**	5.15	1.897	0.225	2.35 e-4	0.649	1.692	0.350	0.469	n/m*	12.1 e-4
Error/%	4.0	8.3	5.5	9.7	20.1	2.1	2.5	0.2	-	
***SC2-d*$_1$**	-	1.123	0.936	1.06 e-5	0.829	2.131	0.646	0.478	n/m*	3.83 e-4
Error/%	-	0.74	1.01	11.75	1.13	1.39	1.67	0.15	-	
***SC3-d*$_1$**	-	1.311	0.486	2.76 e-5	0.857	2.354	0,372	0,462	383.1	3.44 e-4
Error/%	-	0.7	1.9	20.4	2.0	1.3	1.7	0.2	17.8	
***SC4-d*$_1$**	-	1.145	2.428	2.35 e-6	0.856	2.833	0.44	0.467	5911	2.98 e-4
Error/%	-	2.1	1.1	8.6	0.9	1.6	2.0	0.2	43.4	

*Not measurable—too high to be determined

Table 6 Results of mathematical fitting of impedance spectra of assembled supercapacitors with different electrode compositions and similar electrode thickness of $d_2 \sim 120$ µm. *CPE-τ* and *CPE-p* represent the parameters that mathematically describe the *CPE* element, while R_S, Z_S-*τ*, and Z_S-*p* represent the Z_S element in the model

	L/H e-8	R_{HF}/Ω	R_1/Ω	*CPE-τ*/Ss^p	*CPE-p*	R_S/Ω	Z_S-*τ*/s	Z_S-*p*	R_2/Ω	χ^2
***SC1-d*$_2$**	7.99	0.938	0.081	0.0124	0.5232	2.664	1.211	0.473	n/m*	2.4 e-4
Error/%	2.6	1.7	22.0	61.9	15.7	0.76	0.99	0.17	-	
***SC2-d*$_2$**	4.65	1.0	0.061	0.331	0.404	3.46	2.0	0.483	8830	2.61 e-4
Error/%	3.0	0.6	16.5	66.9	21.1	0.81	1.0	0.2	18.3	
***SC3-d*$_2$**	6.88	1.1	0.093	0.366	0.359	3.844	2.478	0.475	n/m*	4.99 e-4
Error/%	4.9	1.2	23.8	74.1	29.0	1.2	1.5	0.2	-	
***SC4-d*$_2$**	-	1.43	7.14	3.91e-6	0.77	2.715	0.553	0.470	n/m*	3.22 e-4
Error/%	-	2.6	0.6	5.5	0.6	3.0	3.4	0.2	-	

*Not measurable—too high to be determined

Effect of the electrode thickness

As might be expected, the thickness of the electrodes has a profound influence on the overall performance of the supercapacitors. The obvious unfavorable effect of increased resistances at thicker electrodes should be partially compensated by higher capacitances supposed to be achieved when the more active material is involved in the charging/discharging reaction. This interplay between resistance and capacitance is the usual challenge that needs to be addressed during supercapacitor design since the optimization of one parameter leads to the deterioration of the other. The low resistances are important for the high-power devices, while the increase of the energy content is in direct correlation with the capacitances. Thus, to optimize the supercapacitor device, the application's requirements should be known.

We investigated the series of AC/AC supercapacitors of various compositions prepared from the electrodes of different thicknesses, usually in the range of 50–200 µm, and typical EIS spectra are depicted in Fig. 9. It is noticeable that all regions of impedance spectra, including R_{HF}, the size of the kinetic semicircle, and low-to-medium-frequency diffusion/capacitance processes are affected by the thickness of the electrode. As expected, the overall capacitance of electrodes and, accordingly, energy storage capability increases with the thickness, i.e., mass of active electrode material. The capacitances obtained by DC charging/discharging of capacitors and by the calculation from the low-frequency impedance are compared in Table 7. Specific capacitance calculated from the charging/discharging process is also given in Table 7. The relative insensitivity of specific capacitance on electrode thickness reveals efficient and complete wetting of the active material in the investigated range of thicknesses what is favorable from the energy storage point of view. However, a total resistance within pores, R_s, depicted as a length of the Warburg region of the transmission line model (Fig. 9 inset and Table 8) increases with the electrode thickness contributing to the power deterioration of the supercapacitor. Assuming complete electrode wetting as discussed previously, electrolyte diffusion and/or migration between particles tend to be equally important for the supercapacitor performance as the diffusion of ions inside the porous structure of the carbon particles. The intersection of the Warburg line and the low-frequency capacitive vertical line occurs at the frequency usually termed as a "knee" frequency which describes the power capability of

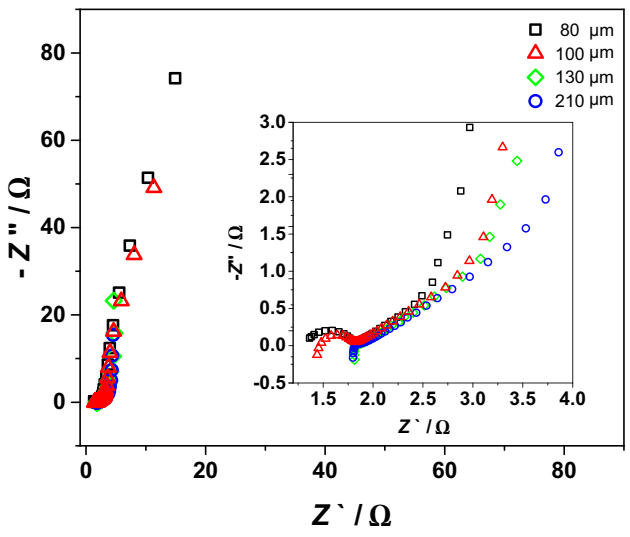

Fig. 9 Nyquist diagram of SC3 supercapacitor with different electrode thickness. In order to observe a length of 45° slope, all curves are fixed at the same R_1 value

Table 7 Comparison of capacity values of SC3 supercapacitor obtained from the fitted parameter Z_S-*τ* (EIS) and the charging /discharging curves (GCD) according to Eq. 3

Electrode thickness, *d* / µm	***C*/F**		***C*$_s$/F g^{-1}** (GCD)
	EIS	**GCD**	
80	0.1582	0.1528	10.7
100	0.2702	0.2279	10.1
130	0.6446	0.5103	13.6
210	0.9917	0.7368	13.4

Table 8 Dependence of total resistance within the pores, R_s, with electrode thickness of SC3 supercapacitor extracted from fitting results of impedance spectra

Electrode thickness, d/μm	R_s/Ω (EIS)
80	2.354
100	3.683
130	3.844
210	5.312

the supercapacitor and is usually called a figure of merit [45]. Generally, the higher the knee frequency, the lower the system's time constant, and the supercapacitor could be discharged at higher power. More explicit way of representation of these data is plots of the imaginary part of the capacitance, $C_{im}(\omega)$ vs. frequency. The imaginary part of the capacitance gives energy loss by the system and is given by Eq. 7.

$$C_{im}(\omega) = \frac{-Z_{re}(\omega)}{\omega|Z(\omega)|^2} \tag{7}$$

The evolution of $C_{im}(\omega)$ for the AC/AC capacitors shown in Fig. 9 goes through the maxima as depicted in Fig. 10. As the electrode thickness increases, observed maxima shift in the direction of lower frequencies, i.e., higher time constants. The energy loss is correlated with the height of the maxima and follows the same direction as the observed time constants, thicker electrodes are able to convert less stored energy into the usable form. The time constants for the investigated electrode thicknesses of 80, 100, 130, and 210 μm are 4.3, 6.2, 14.3, and 20.0 s, respectively.

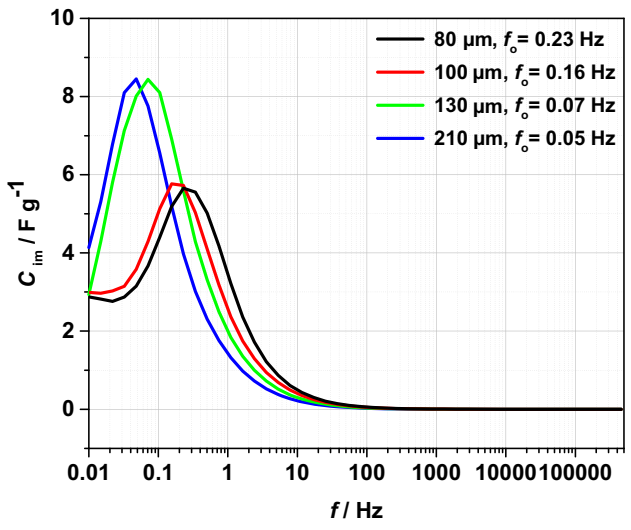

Fig. 10 Plots of imaginary capacitance as a function of frequency for SC3 supercapcitor with different electrode thickness. The f_o represents the maxima of imaginary capacitance

Conclusions

In this study, new results about the influence of active electrode content on the supercapacitor performance were demonstrated. The results enhance the existing knowledge about the active carbon behavior, especially about the minute influence of electrode composition of the frequency responses of supercapacitor electrodes. Apart from the high-frequency inductive region of the impedance plots, all three regions, middle-frequency kinetic semicircle and low-frequency diffusion/capacitive behavior of porous electrodes, are highly sensitive to the electrode composition. High-frequency inductive behavior is not related to the physical process in the supercapacitor, but it is essential to take it into account during modeling and fitting of experimental data to accurately predict high-frequency resistance.

The application of the external pressure on the supercapacitor cell revealed that (i) the high-frequency semicircle originates from the kinetic effects on the current collector/carbon solid/solid interphase and (ii) microporous structure of carbon material was not affected by the applied pressure and complete wetting of the interior of carbon pores was achieved by the preparation procedures undertaken in this work.

The influence of the electrode composition on the impedance spectra is reflected in both the low-frequency capacitive range and in the high-frequency kinetic region, while high-frequency resistance remains largely insensitive to the change in the content of the individual components. Sometimes the effects of the individual components oppose each other, making the quantification of these effects difficult. PVDF as a binder has a positive influence on the diminishing impedance at high frequencies due to improving interparticle contacts on the electrode. Thus, both carbon black providing conductive paths through the electrode layer and PVDF providing mechanical integrity of the electrode, improving interparticle contacts, play an important role in ensuring good conductivity of the layers and in diminishing the charge transfer at the interfaces. On the other hand, in the low-frequency region, PVDF increases the impedance due to the blocking of the porous structure of the carbon particles. The optimal PVDF content of 10% was found in this work.

The results indicate that the charge transfer at the current collector/active material interface occurs via the electron exchange with the active carbon and the electron transfer to carbon black could be neglected.

Acknowledgements The support of Croatian Science Foundation under the project ESUP-CAP (IP-11-2013-8825) is greatly acknowledged.

Funding Hrvatska Zaklada za Znanost, IP-11–2013-8825, Zoran Mandic.

Declarations

Conflict of interest The authors declare no competing interests.

References

1. Simon P, Gogotsi Y (2008) Materials for electrochemical capacitors. Nat Mater 7:845–854. https://doi.org/10.1038/nmat2297
2. Naoi K, Simon P (2008) New materials and new confgurations for advanced electrochemical capacitors. Electrochem Soc Interface 17:34–37. https://doi.org/10.1149/2.f04081if
3. Salanne M, Rotenberg B, Naoi K et al (2016) Efficient storage mechanisms for building better supercapacitors. Nat Energy 1:16070. https://doi.org/10.1038/nenergy.2016.70
4. Zhang Y, Ru Y, Gao HL et al (2019) Sol-gel synthesis and electrochemical performance of $NiCo_2O_4$ nanoparticles for supercapacitor applications. J Electrochem Sci Eng 9:243–253. https://doi.org/10.5599/jese.690
5. Yu X, Li B (2019) In-situ synthesis of mesoporous carbon/iron sulfide nanocomposite for supercapacitors. J Electrochem Sci Eng 9:55–62. https://doi.org/10.5599/jese.572
6. Yadav M (2020) Metal oxides nanostructure-based electrode materials for supercapacitor application. J Nanoparticle Res 22. https://doi.org/10.1007/s11051-020-05103-2
7. Liu R, Zhou A, Zhang X et al (2021) Fundamentals, advances and challenges of transition metal compounds-based supercapacitors. Chem Eng J 412:128611. https://doi.org/10.1016/j.cej.2021.128611
8. Naskar P, Maiti A, Chakraborty P et al (2021) Chemical supercapacitors: a review focusing on metallic compounds and conducting polymers. J Mater Chem A 9:1970–2017. https://doi.org/10.1039/D0TA09655E
9. Holze R (2020) Composites and copolymers containing redox-active molecules and intrinsically conducting polymers as active masses for supercapacitor electrodes—an introduction. Polymers 12:1835. https://doi.org/10.3390/polym12081835
10. Kong J, Yue Q, Wang B et al (2013) Short communication. J Anal Appl Pyrolysis 104:710–713. https://doi.org/10.1016/j.jaap.2013.05.024
11. Lee H-M, Kim TA H-G, An K-H, Śliwak A (2014) Effects of pore structures on electrochemical behaviors of polyacrylonitrile-based activated carbon nanofibers by carbon dioxide activation. Carbon Lett 15:71–76.https://doi.org/10.5714/CL.2014.15.1.071
12. Roh JS (2003) Microstructural changes during activation process of isotopic carbon fibers using CO_2 Gas(I)-XRD Study. Korean J Mater Res 13:742–748. https://doi.org/10.3740/MRSK.2003.13.11.742
13. Fu K, Yue Q, Gao B et al (2013) Preparation, characterization and application of lignin-based activated carbon from black liquor lignin by steam activation. Chem Eng J 228:1074–1082. https://doi.org/10.1016/j.cej.2013.05.028
14. Bang JH, Lee HM, An KH, Kim BJ (2017) A study on optimal pore development of modified commercial activated carbons for electrode materials of supercapacitors. Appl Surf Sci 415:61–66. https://doi.org/10.1016/j.apsusc.2017.01.007
15. Ruiz V, Blanco C, Granda M et al (2007) Influence of electrode preparation on the electrochemical behaviour of carbon-based supercapacitors. J Appl Electrochem 37:717–721. https://doi.org/10.1007/s10800-007-9305-5
16. Li Y, Pu Z, Sun Q, Pan N (2021) A review on novel activation strategy on carbonaceous materials with special morphology/texture for electrochemical storage. J Energy Chem 60:572–590. https://doi.org/10.1016/j.jechem.2021.01.017
17. Rajaputra SS, Pennada N, Yerramilli A, Kummara NM (2021) Graphene based sulfonated polyvinyl alcohol hydrogel nanocomposite for flexible supercapacitors. J Electrochem Sci Eng 11:197–207. https://doi.org/10.5599/JESE.1031
18. Pang Z, Li G, Xiong X et al (2021) Molten salt synthesis of porous carbon and its application in supercapacitors: a review. J Energy Chem 61:622–640. https://doi.org/10.1016/j.jechem.2021.02.020
19. Wen Y, Kok MDR, Tafoya JPV et al (2021) Electrospinning as a route to advanced carbon fibre materials for selected low-temperature electrochemical devices: a review. J Energy Chem 59:492–529. https://doi.org/10.1016/j.jechem.2020.11.014
20. Sačer D, Spajić I, Kraljić Roković M, Mandić Z (2018) New insights into chemical and electrochemical functionalization of graphene oxide electrodes by o-phenylenediamine and their potential applications. J Mater Sci 53:15285–15297. https://doi.org/10.1007/s10853-018-2693-6
21. Lee SJ, Theerthagiri J, Nithyadharseni P et al (2021) Heteroatom-doped graphene-based materials for sustainable energy applications: a review. Renew Sustain Energy Rev 143:110849. https://doi.org/10.1016/j.rser.2021.110849
22. Liu P, Verbrugge M, Soukiazian S (2006) Influence of temperature and electrolyte on the performance of activated-carbon supercapacitors. J Power Sources 156:712–718. https://doi.org/10.1016/j.jpowsour.2005.05.055
23. Chmiola J, Yushin G, Gogotsi Y et al (2006) Anomalous increase in carbon at pore sizes less than 1 nanometer. Science 313:1760–1763. https://doi.org/10.1126/science.1132195
24. Raymundo-Piñero E, Kierzek K, Machnikowski J, Béguin F (2006) Relationship between the nanoporous texture of activated carbons and their capacitance properties in different electrolytes. Carbon 44:2498–2507. https://doi.org/10.1016/j.carbon.2006.05.022
25. Mysyk R, Raymundo-Piñero E, Pernak J, Béguin F (2009) Confinement of symmetric tetraalkylammonium ions in nanoporous carbon electrodes of electric double-layer capacitors. J Phys Chem C 113:13443–13449. https://doi.org/10.1021/jp901539h
26. Lozano-Castelló D, Cazorla-Amorós D, Linares-Solano A et al (2003) Influence of pore structure and surface chemistry on electric double layer capacitance in non-aqueous electrolyte. Carbon 41:1765–1775. https://doi.org/10.1016/S0008-6223(03)00141-6
27. Kim I-T, Egashira M, Yoshimoto N, Morita M (2011) On the electric double-layer structure at carbon electrode/organic electrolyte solution interface analyzed by ac impedance and electrochemical quartz-crystal microbalance responses. Electrochim Acta 56:7319–7326. https://doi.org/10.1016/j.electacta.2011.06.044
28. Ohta T, Kim IT, Egashira M et al (2012) Effects of electrolyte composition on the electrochemical activation of alkali-treated soft carbon as an electric double-layer capacitor electrode. J Power Sources 198:408–415. https://doi.org/10.1016/j.jpowsour.2011.10.006
29. Vix-Guterl C, Frackowiak E, Jurewicz K et al (2005) Electrochemical energy storage in ordered porous carbon materials. Carbon 43:1293–1302. https://doi.org/10.1016/j.carbon.2004.12.028
30. Chmiola J, Largeot C, Taberna P-L et al (2008) Desolvation of ions in subnanometer pores and its effect on capacitance and double-layer theory. Angew Chemie Int Ed 47:3392–3395. https://doi.org/10.1002/anie.200704894
31. Decaux C, Matei Ghimbeu C, Dahbi M et al (2014) Influence of electrolyte ion–solvent interactions on the performances of supercapacitors porous carbon electrodes. J Power Sources 263:130–140. https://doi.org/10.1016/j.jpowsour.2014.04.024
32. Mecklenfeld A, Raabe G (2020) GAFF/IPolQ-Mod+LJ-Fit: Optimized force field parameters for solvation free energy predictions. ADMET DMPK 8:274–296. https://doi.org/10.5599/admet.837

33. Dobrota AS, Pašti IA (2020) Chemisorption as the essential step in electrochemical energy conversion. J Electrochem Sci Eng 10:141–159. https://doi.org/10.5599/jese.742
34. Tsay KC, Zhang L, Zhang J (2012) Effects of electrode layer composition/thickness and electrolyte concentration on both specific capacitance and energy density of supercapacitor. Electrochim Acta 60:428–436. https://doi.org/10.1016/j.electacta.2011.11.087
35. Abbas Q, Pajak D, Frąckowiak E, Béguin F (2014) Effect of binder on the performance of carbon/carbon symmetric capacitors in salt aqueous electrolyte. Electrochim Acta 140:132–138. https://doi.org/10.1016/jelectacta2014.04.096
36. Daraghmeh A, Hussain S, Servera L et al (2017) Impact of binder concentration and pressure on performance of symmetric CNFs based supercapacitors. Electrochim Acta 245:531–538. https://doi.org/10.1016/j.electacta.2017.05.186
37. MA, Paul A (2017) Importance of electrode preparation methodologies in supercapacitor applications. ACS Omega 2:8039–8050. https://doi.org/10.1021/acsomega.7b01275
38. Tran HY, Wohlfahrt-Mehrens M, Dsoke S (2017) Influence of the binder nature on the performance and cycle life of activated carbon electrodes in electrolytes containing Li-salt. J Power Sources 342:301–312. https://doi.org/10.1016/j.jpowsour.2016.12.056
39. Varzi A, Passerini S (2015) Enabling high areal capacitance in electrochemical double layer capacitors by means of the environmentally friendly starch binder. J Power Sources 300:216–222. https://doi.org/10.1016/j.jpowsour.2015.09.065
40. Varzi A, Raccichini R, Marinaro M et al (2016) Probing the characteristics of casein as green binder for non-aqueous electrochemical double layer capacitors' electrodes. J Power Sources 326:672–679. https://doi.org/10.1016/j.jpowsour.2016.03.072
41. Lufrano F, Staiti P, Minutoli M (2004) Influence of Nafion content in electrodes on performance of carbon supercapacitors. J Electrochem Soc 151:A64. https://doi.org/10.1149/1.1626670
42. Yamagata M, Ikebe S, Soeda K, Ishikawa M (2013) Ultrahigh-performance nonaqueous electric double-layer capacitors using an activated carbon composite electrode with alginate. RSC Adv 3:1037–1040. https://doi.org/10.1039/C2RA22188H
43. Sopčić S, Antonić D, Mandić Z et al (2018) Single and multi-frequency impedance characterization of symmetric activated carbon single capacitor cells. J Electrochem Sci Eng 8:183–195. https://doi.org/10.5599/jese.536
44. Kötz R, Carlen M (2000) Principles and applications of electrochemical capacitors. Electrochim Acta 45:2483–2498. https://doi.org/10.1016/S0013-4686(00)00354-6
45. Taberna PL, Simon P, Fauvarque JF (2003) Electrochemical characteristics and impedance spectroscopy studies of carbon-carbon supercapacitors. J Electrochem Soc 150:A292. https://doi.org/10.1149/1.1543948
46. De Levie R (1967) Electrochemical response of porous and rough electrodes. Adv Electrochem Electrochem Eng 6:329–397
47. Pohlmann S, Lobato B, Centeno TA, Balducci A (2013) The influence of pore size and surface area of activated carbons on the performance of ionic liquid based supercapacitors. Phys Chem Chem Phys 15:17287–17294. https://doi.org/10.1039/C3CP52909F
48. Petrić V, Mandić Z (2021) On the need for simultaneous electrochemical testing of positive and negative electrodes in carbon supercapacitors. Electrochim Acta 384:138372. https://doi.org/10.1016/j.electacta.2021.138372
49. Balducci A (2016) Electrolytes for high voltage electrochemical double layer capacitors: A perspective article. J Power Sources 326:534–540. https://doi.org/10.1016/j.jpowsour.2016.05.029
50. Pal B, Yang S, Ramesh S et al (2019) Electrolyte selection for supercapacitive devices: a critical review. Nanoscale Adv 1:3807–3835. https://doi.org/10.1039/c9na00374f
51. Han J, Yoshimoto N, Todorov YM et al (2018) Characteristics of the electric double-layer capacitors using organic electrolyte solutions containing different alkylammonium cations. Electrochim Acta 281:510–516. https://doi.org/10.1016/j.electacta.2018.06.012
52. Koh AR, Hwang B, Chul Roh K, Kim K (2014) The effect of the ionic size of small quaternary ammonium BF4 salts on electrochemical double layer capacitors. Phys Chem Chem Phys 16:15146–15151. https://doi.org/10.1039/c4cp00949e
53. Arulepp M, Permann L, Leis J et al (2004) Influence of the solvent properties on the characteristics of a double layer capacitor. J Power Sources 133:320–328. https://doi.org/10.1016/j.jpowsour.2004.03.026
54. CENELEC (2012) Electric double-layer capacitors for use in hybrid electric vehicles – Test methods for electrical characteristics (IEC 62576:2009; EN 62576:2010) Na
55. Delacourt C, Ridgway PL, Srinivasan V, Battaglia V (2014) Measurements and simulations of electrochemical impedance spectroscopy of a three-electrode coin cell design for Li-ion cell testing. J Electrochem Soc 161:A1253–A1260. https://doi.org/10.1149/2.0311409jes
56. Murer N, Diard JP, Petrescu B (2020) The effects of time-variance on impedance measurements: examples of a corroding electrode and a battery cell. J Electrochem Sci Eng 10:127–140. https://doi.org/10.5599/jese.725
57. Sugano K (2021) Lost in modelling and simulation? ADMET DMPK 9:75–109. https://doi.org/10.5599/admet.923
58. Avdeef A (2021) Do you know your r2? ADMET DMPK J 9:69–74
59. Kaus M, Kowal J, Sauer D (2010) Modelling the effects of charge redistribution during self-discharge of supercapacitors. Electrochim Acta 55:7516–7523. https://doi.org/10.1016/j.electacta.2010.01.002
60. Kowal J, Avaroglu E, Chamekh F et al (2011) Detailed analysis of the self-discharge of supercapacitors. J Power Sources 196:573–579. https://doi.org/10.1016/j.jpowsour.2009.12.028
61. Roberts AJ, Slade RCT (2010) Effect of specific surface area on capacitance in asymmetric carbon/α-MnO_2 supercapacitors. Electrochim Acta 55:7460–7469. https://doi.org/10.1016/j.electacta.2010.01.004
62. Ruiz V, Blanco C, Santamaría R et al (2009) An activated carbon monolith as an electrode material for supercapacitors. Carbon 47:195–200. https://doi.org/10.1016/j.carbon.2008.09.048
63. EC-Lab – Application Note (2017) # 62 How to measure the internal resistance of a battery using EIS ? 1–6
64. Moškon J, Talian SD, Dominko R, Gaberšček M (2020) Advances in understanding li battery mechanisms using impedance spectroscopy. J Electrochem Sci Eng 10:79–93. https://doi.org/10.5599/jese.734
65. Dsoke S, Tian X, Täubert C et al (2013) Strategies to reduce the resistance sources on electrochemical double layer capacitor electrodes. J Power Sources 238:422–429. https://doi.org/10.1016/j.jpowsour.2013.04.031
66. Allagui A, Freeborn TJ, Elwakil AS, Maundy BJ (2016) Reevaluation of performance of electric double-layer capacitors from constant-current charge/discharge and cyclic voltammetry. Sci Rep 6:38568. https://doi.org/10.1038/srep38568
67. Batalla García B, Feaver AM, Zhang Q et al (2008) Effect of pore morphology on the electrochemical properties of electric double layer carbon cryogel supercapacitors. J Appl Phys 104:14305. https://doi.org/10.1063/1.2949263
68. Karden E, Buller S, De Doncker RW (2002) A frequency-domain approach to dynamical modeling of electrochemical power sources. Electrochim Acta 47:2347–2356. https://doi.org/10.1016/S0013-4686(02)00091-9
69. Atebamba J-M, Moskon J, Pejovnik S, Gaberscek M (2010) On the interpretation of measured impedance spectra of insertion cathodes for lithium-ion batteries. J Electrochem Soc 157:A1218. https://doi.org/10.1149/1.3489353
70. Gaberšček M, Moškon J, Erjavec B et al (2008) The importance of interphase contacts in li ion electrodes: the meaning of the

high-frequency impedance arc. Electrochem Solid-State Lett 11:A170. https://doi.org/10.1149/1.2964220
71. Li X, Rong J, Wei B (2010) Electrochemical behavior of single-walled carbon nanotube supercapacitors under compressive stress. ACS Nano 4:6039–6049. https://doi.org/10.1021/nn101595y